JOURNAL OF SYNCHROTRON RADIATION

ISSN 1600-5775

High-pressure and -temperature spinning capillary cell for *in situ* synchrotron X-ray powder diffraction

Edmundo Fraga,[a,b] Jesus D. Zea-Garcia,[c] Armando Yáñez,[b] Angeles G. De la Torre,[c] Ana Cuesta,[c] Ricardo Valcárcel-Fernández,[a] Francesc Farré-París,[a] Marc Malfois[a] and Miguel A. G. Aranda[a,c]*

[a]ALBA Synchrotron, Carrer de la Lum 2-26, 08290 Cerdanyola del Vallès, Barcelona, Spain, [b]Departamento de Ingeniería Naval e Industrial, Universidade da Coruña, Campus de Esteiro S/N, 15403 Ferrol, A Coruña, Spain, and [c]Departamento de Química Inorgánica, Universidad de Málaga, Campus Teatinos S/N, 29071 Málaga, Spain. *Correspondence e-mail: migarcia@cells.es

Received 11 December 2018
Accepted 15 April 2019

Edited by V. Favre-Nicolin, CEA and Université Joseph Fourier, France

Keywords: high-pressure equipment; oil well cement; cement hydration; Rietveld quantitative phase analysis.

Supporting information: this article has supporting information at journals.iucr.org/s

In situ research of materials under moderate pressures (hundreds of bar) is essential in many scientific fields. These range from gas sorption to chemical and biological processes. One industrially important discipline is the hydration of oil well cements. Existing capillary cells in this pressure range are static as they are easy to design and operate. This is convenient for the study of single-phase materials; however, powder diffraction quantitative analyses for multiphase systems cannot be performed accurately as a good powder average cannot be attained. Here, the design, construction and commissioning of a cost-effective spinning capillary cell for *in situ* powder X-ray diffraction is reported, for pressures currently up to 200 bar. The design addresses the importance of reducing the stress on the capillary by mechanically synchronizing the applied rotation power and alignment on both sides of the capillary while allowing the displacement of the supports needed to accommodate different capillaries sizes and to insert the sample within the tube. This cell can be utilized for multiple purposes allowing the introduction of gas or liquid from both ends of the capillary. The commissioning is reported for the hydration of a commercial oil well cement at 150 bar and 150°C. The quality of the resulting powder diffraction data has allowed *in situ* Rietveld quantitative phase analyses for a hydrating cement containing seven crystalline phases.

1. Introduction

Sample environments specifically designed for *in situ* powder synchrotron X-ray diffraction studies under high pressure and temperature are essential in many research fields. These scientific areas include gas sorption of many kinds, chemical and biological reactions, and characterization of materials behaviour, which have all been extensively discussed (Jupe & Wilkinson, 2006; Hansen *et al.*, 2015; Sakaki *et al.*, 2018). These capillary cells, which allow *in situ* studies in the hundreds of bar region, are static and allow to characterize the structural changes of a single phase under different gases (Hansen *et al.*, 2015; Sakaki *et al.*, 2018) or to follow the phase development in hydrating oil well cements (Jupe & Wilkinson, 2006).

However, with static cells, powder diffraction quantitative studies for multiphase systems cannot be performed properly as a good powder average cannot be attained. Ensuring good particle averaging is essential for the study of several commercially relevant systems like oil well cement hydration. The relevance of spinning the samples in powder diffraction, and its implication for particle statistics, has been already discussed (Ida *et al.*, 2009).

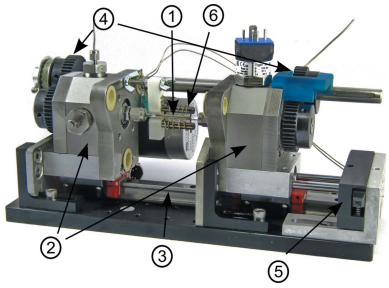

For capillary cells, also known as microreactors, there is an intermediate possibility. It is common practice to increase the particle statistics, in the volume probed by the X-rays, by rocking the cell by 5–10° on its axis. A review of capillary cells has recently been published, containing key references dealing with rocking cells (van Beek & Pattison, 2018).

Synchrotron radiation is especially useful for the *in situ* characterization of processes because it is possible to select an X-ray beam of high energy (enables penetration) with very high flux (permits good signal-to-noise ratio). A review focused on the uses of synchrotron techniques for the study of building materials has been already published (Aranda, 2016). This paper is framed within our research efforts to characterize *in situ* cement hydration by synchrotron techniques. Here, we report the development of a spinning capillary cell which allows *in situ* Rietveld quantitative phase analyses of hydrating cements. Furthermore, this cell can be easily adapted for gas sorption studies by swapping the pressure-transmitting agent from oil to the appropriate gas.

2. Materials and methods

2.1. Spinning capillary cell

2.1.1. General description.. The cell is composed of a high-pressure-resistant capillary, where the sample is loaded; two side supports to connect the rotating capillary to the pressure-measurement system and the pressure mean; a linear displacement system to be able to accommodate different capillary sizes and to access the interior of the capillary to change the sample; a transmission system which applies the rotation power to the capillary; a spring lock system to automatically lock the system before applying pressure; and a heating system to reach the target temperature. The main components of this cell are sketched in Fig. 1. The 3D design is shown in Fig. S1 of the supporting information.

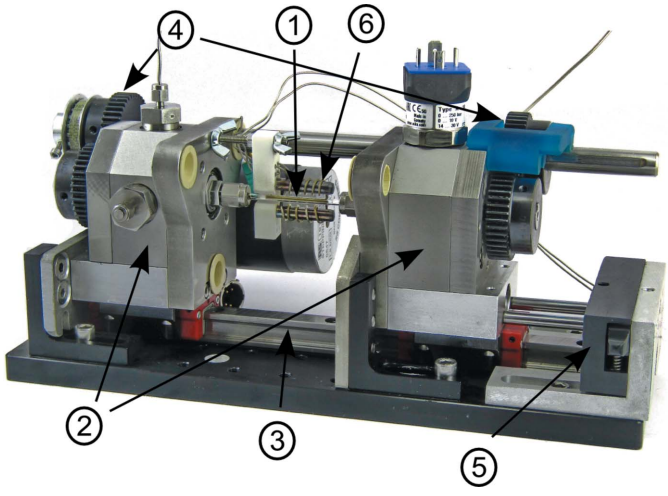

Figure 1
Photograph of the spinning cell with its main components. 1: Sample holder (removable capillary); 2: side supports; 3: linear displacement system; 4: transmission system; 5: spring lock system; 6: heating system.

2.1.2. Sample holder. For this commissioning study, the sample holders are 'single crystal' sapphire capillaries supplied by Saint-Gobain Crystals. These capillaries are grown along the *c*-axis direction, the (0001) plane. The outer and inner diameters of the sapphire tubes are 3.18 mm and 1.75 mm, respectively. It is difficult to estimate the rupture stress defects for such a small single crystal as defects and micro-fractures vary considerably and are the main source of fracture. According to the manufacturer, these capillaries can handle pressures up to around 550 bar with 2× factor of safety at room temperature. However, as discussed by Azhdari *et al.* (1998), different crystallographic planes have different surface energies, *i.e.* the planes $(1\bar{1}02)$ and $(11\bar{2}3)$, with low fracture surface energies, will support more sheer stresses under the torque needed for rotation. Other materials for capillaries (titanium or steel) can withstand higher pressures, but it is necessary to use higher-energy synchrotron radiation in order to penetrate these metal tubes.

The relation between the ultimate tensile strength of sapphire and the burst pressure for thin-walled capillaries has been studied (Jensen *et al.*, 2010). For sapphire capillaries of 1.09 mm outer diameter and 0.79 mm inner diameter, supplied by Saint-Gobain Crystals, the burst pressure was measured to be 900 bar. It was also stated that capillaries from another manufacturer, of lower quality, burst at a much lower pressure. A wider discussion on this topic has recently been reported by the same group (Hansen *et al.*, 2015).

When using sapphire it is essential to reduce the torque on the capillary. This was done by avoiding any misalignment on both sides of the supporting axis, and synchronizing the torque applied on both sides leaving only a low amount of inertia torque that will be reduced with long (slow) accelerations.

2.1.3. Side supports. The capillary is supported on two shafts made from AISI310 stainless steel, which is known to have good strength and good resistance to corrosion and oxidation at elevated temperatures and pressures. One of its ends has a two-ferrule tube compression fitting of size 1/8. The ferrules are made of a mixture of polyimide and graphite (Teide from Teknokroma), selected due to their capabilities to seal against sapphire with little force and so avoiding any extra stress on the capillary. A hole in the centre of the axis reaches the middle, giving access to the main pressure-exchanger chamber where the pressure mean, or the sample in the case of continuous flow, enters into the axis. On the other end, the axis has an adaptor to install a carbon steel spur gear (SS1-40C from KHK) with 40 teeth, module 1, and an inner diameter of 12 mm that will drive the spinning.

The axis is mounted in an asymmetric-bearing cross-located design with two angular contact ball bearings in back-to-back configuration. The intention is to have a located axis that will not move under different pressures and have a large front bearing that can accommodate the rotation radial loads and axial loads from the pressure forces and channel them to the main support. This inner bearing, the closest to the sample, is a single-row angular contact ball bearing (7200BEP from SKF); this kind of bearing can support normal axial loads at high

speeds and channel the force to the main support. The main components of the side supports are depicted in Fig. 2.

The support body is the exchanger part and has two pressure entrances; one is used to transmit the pressure to the exchanger chamber and the other one can be used to measure the pressure inside that chamber. The direct pressure measurement system (A-10 from WIKA) inside this exchanger chamber assures that the pressure is transmitted into the capillary, as it is connected by four holes and an unlikely blockage in one hole would have negligible effect. The axis is sealed with two PTFE seals (FlexiSeal with a FLO profile from PARKER), as they are suitable for both liquids and gases, and the pressure range of application goes up to 200 bar and from −260°C to +315°C in temperature.

2.1.4. Linear displacement system. The two side supports are installed in two Schneeberger carriages that run into a linear ball guides monorail with the highest accuracy range, from the manufacturer G0; these ensure minimum vertical and horizontal deviations in parallelism in the carriages while moving over the guide rail. This, together with the restricted tolerances in dimensions and parallelism used to manufacture the support, results in a high degree of collinearity in both axes, one of the conditions needed to avoid stress on the capillary and especially the very dangerous combinations of rotation and bending momentums that can lead to fracture by fatigue.

2.1.5. Transmission system. The transmission consists of a 12 mm shaft driven by a stepper motor through a pulley transmission. This shaft is connected to the main axes by two carbon steel spur gears with 40 teeth, module 1. The connection is made with a key system that prevents relative rotation and assures the same position of the gears, having a synchronizing movement in both sides of the capillary; on top of that, one of the two train gears can be displaced into the driving shaft while the key systems disable the rotation. This approach allows the cell to be quickly opened and closed to access the inside of the capillary for sample exchange while maintaining the tooth synchronization on both sides. Spinning is always in the same direction to avoid backlash on the tooth contact. Here, long accelerations times are used, around 10 s to reach a speed of 250 revolutions per minute (r.p.m.), to minimize mechanical stress. The components of the transmission system are depicted in Fig. 3.

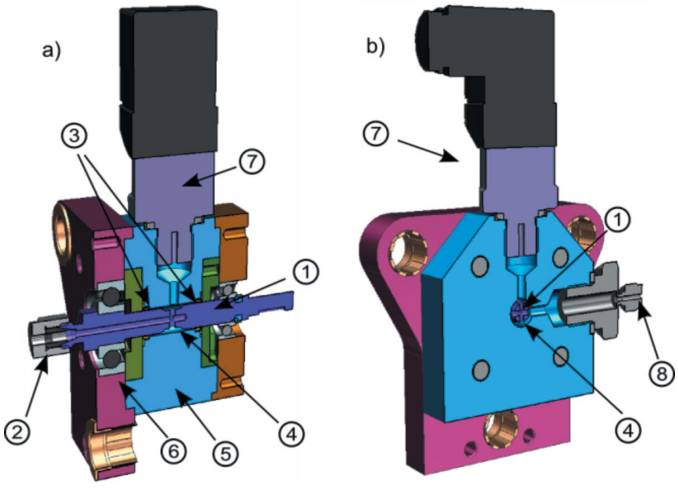

Figure 2
Cross sections of the side supports. (*a*) Longitudinal view. (*b*) Transversal view. 1: Main shaft; 2: tube compression fitting system; 3: PTFE seals; 4: exchanger chamber; 5: support body; 6: front bearing; 7: pressure measurement; 8: pressure inlet.

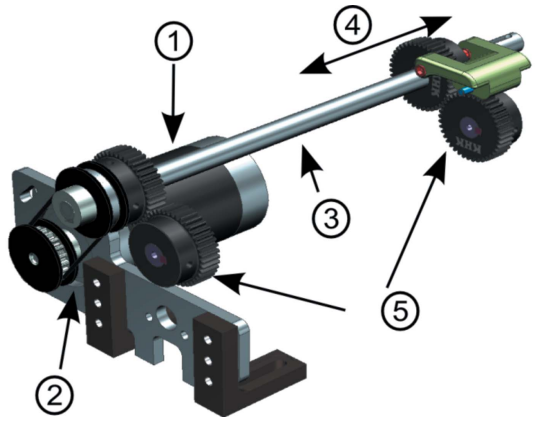

Figure 3
Transmission system. 1: 2-Phase hybrid stepper motor with a holding torque 1.2 N m; 2: metric timing pulleys system t5 pitch; 3: main 12 mm transmission shaft; 4: horizontal geared displacements; 5: spur gears system, module 1, 40 teeth and precision grade N8.

2.1.6. Spring lock system. The cell has an automatic spring lock system enabling a quick change of the sample and as a safety system to avoid movement of the carriages in the rail. When the capillary size is adjusted, movement of the carriages to open/close is automatically locked without needing to be fixed by any other method.

2.1.7. Pressure generator by oil. For the case under discussion here, *i.e.* hydration of cements, static pressure was produced with equipment similar to that reported by Jupe & Wilkinson (2006), containing a mineral light white oil pressure-transmitting medium (Kaydol-type from Sigma-Aldrich). The pressure is generated by a manual pump generator (HiP) in the range 0–2000 bar. For safety reasons, the pressure-generator assembly is equipped with a rupture disc for overpressure protection. In the existing configuration, the rupture disc is set at 200 bar. The system has a pressure transducer (HP-2 from WIKA) to enable pressure measurement in the generator with a range 0–2500 bar together with a pressure gauge, and it is connected to the cell using a 1/16 inch stainless steel capillary tube with an outside diameter of 1/16 inch. The components of the pressure generator are depicted in Fig. 4.

For gas sorption experiments, the pressure-generator system should be exchanged with gas pressure equipment. As the capillary is accessible from both sides, implementing gas loading is straightforward, for non-hazardous gases.

2.1.8. Heating system. The heating system consists of a resistive 1.2 mm Inconel-sheathed Thermocoax heating wire wrapped around a stainless steel 6 mm rod and mounted into a Macor holding frame (Chupas *et al.*, 2008). The temperature inside the capillary is monitored with a K-type thermocouple

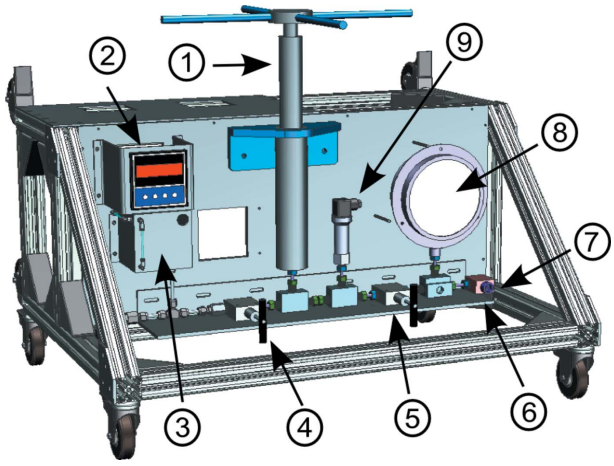

Figure 4
Pressure generator. 1: Manual pressure pump generators; 2: digital pressure display; 3: oil tank at atmospheric pressure; 4: inlet high-pressure valve; 5: outlet high-pressure valve; 6: rupture disc for overpressure protection; 7: outlet to the cell; 8: pressure gauge; 9: pressure transducer.

positioned in the Macor frame and calibrated to compensate for the offset between both positions. The resistance is powered by a power supply connected to a Eurotherm Nanodac that records both the pressure and temperature and has a PID control.

To evaluate the possible impact of deformation due to the pressure forces and also to check the static stresses in the system, a finite-element structural analysis (FEA) was carried out using a Siemens NX Nastran 11 (Sol101) linear solver. Under a pressure of 20 MPa (200 bar) a maximum equivalent tensile stress of 154.92 MPa was found, below the yield strength limit of 200 MPa for AISI 301. A horizontal nodal displacement under 6 µm should not affect the alignment, and an irrelevant vertical displacement under 1 µm would have a negligible effect on the misalignments of both side axes. The results of the FEA study are given in Figs. S2 and S3 of the supporting information.

Alternatively, and if it is more appropriated for the experiment, a hot air blower can be used instead of the resistive system.

2.2. Synchrotron X-ray experiment

The cell-commissioning synchrotron experiment was carried out using the recently upgraded NCD-SWEET beamline at ALBA synchrotron (González *et al.*, 2018). Powder diffraction data were collected in Debye–Scherrer (transmission) configuration employing a beam of size 0.8 mm (vertical) × 1.2 mm (horizontal), and a photon energy of 20 keV (λ = 0.62278 Å) selected with a Si(111) channel-cut crystal monochromator. A Rayonix LX255-HS charge-coupled detector was used (with a pixel size of 44 µm), placed at 313 mm from sample, with a vertical angle tilt of 28.92°. The active image area was 85 mm × 255 mm (h × v). Two-dimensional data were collected in five different positions along the capillary with an interval of 0.5 mm and an exposure time of 2 s per individual pattern.

The cell was rotated at 240 r.p.m., so the sample experienced two full rotations per exposure time. Horizontal movement was made with a Micos LS-180 translation stage, part of the beamline equipment and installed just underneath the cell. The raw diffraction data recorded for the empty sapphire capillary (static and under rotation) are displayed in Fig. S4. Fig. S5 shows the calculated positions for the 2D corundum pattern with the Miller indices. Figs. S4 and S5 show that the diffraction peaks from the cell are well localized on the detector. Therefore, the spots will be masked for the operation and normal azimuthal integration will be performed (see below). For this commissioning experiment, the diffraction peaks from sapphire were simply removed from the 1D patterns.

The 2D data were reduced to 1D data using *pyFAI* software (Ashiotis *et al.*, 2015). The system was calibrated by using a capillary filled with quartz as standard. The 2D raw diffraction images of this standard, both static and under rotation, are given in Fig. S6.

2.3. Powder diffraction data analysis

Powder patterns were analysed by using the *GSAS* suite of programs (Von Dreele & Larson, 2004) to obtain Rietveld quantitative phase analyses (RQPA). Final global optimized parameters were: background coefficients, zero-shift error, cell parameters and peak shape parameters using a pseudo-Voigt function (Thompson *et al.*, 1987).

2.4. Oil well cement and paste preparation

Commercial Oil Well Portland cement Class G HSR (Dyckerhoff-Lengerich, Germany) with a Blaine parameter of 340 $m^2\ kg^{-1}$ was used. Mineralogical composition was determined by RQPA by analysing a laboratory X-ray powder pattern collected with Mo $K\alpha_1$ in a D8 Advance (Bruker) at Servicios Centrales de Apoyo a la investigación (SCAI), University of Malaga, Spain (León-Reina *et al.*, 2016). The laboratory Rietveld fitted pattern is displayed in Fig. S7, with the cement phase analysis reported in the inset.

Cement slurry was prepared by mixing the sample with the corresponding amount of water (water/cement mass ratio equal to 0.47) by hand in a small plastic beaker for 2 min. After that, the paste was immediately loaded into the sapphire capillaries with a syringe and a short piece of silicone tubing. Both ends of the capillaries were blocked with PTFE cylindrical plugs of length 2 mm and outside diameter 1.75 mm (with tolerance for its width smaller than 0.1 mm).

3. Results and discussion

The spinning cell has been commissioned for measuring the hydration of a commercial oil well cement. These cements are used by the oil industry to support metal oil-well liners and to form a gas-tight seal between the bore wall and the liner. The hydration process occurs deep in the ground and is subjected to elevated pressures and temperatures that depend on the characteristics of the field application. This cell is intended to

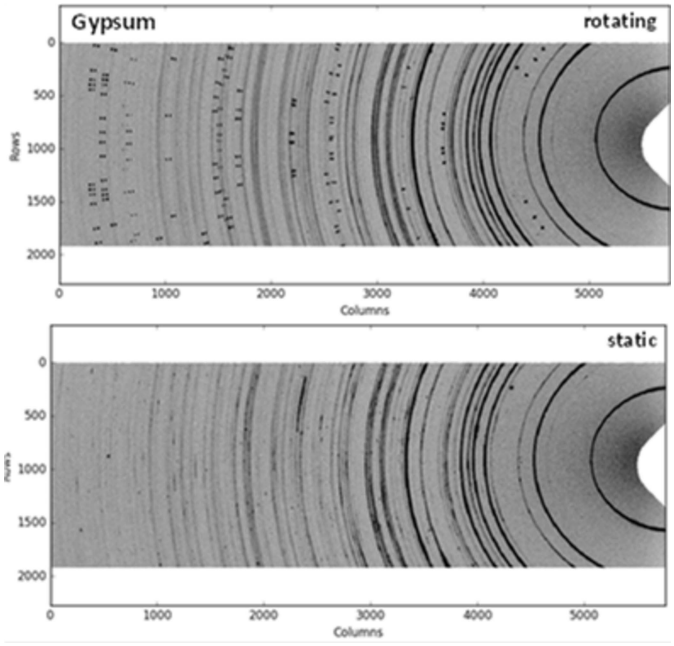

Figure 5
2D synchrotron powder diffraction patterns of the capillary filled with gypsum at room temperature and pressure: (top) rotating and (bottom) static. Diffraction spots from the sapphire are evident in the top pattern and they were masked in the 1D analysis. Note also that sapphire diffraction peaks are split because the two walls of the capillaries are at different distances to the detector.

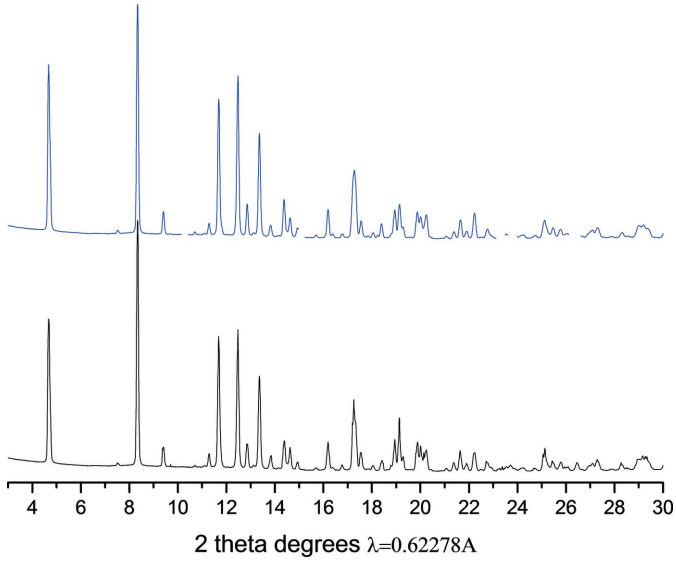

Figure 6
1D synchrotron powder diffraction patterns for gypsum at room temperature and pressure: (top) under rotation and (bottom) static.

reproduce these conditions although access to higher pressures would be clearly advantageous.

After the calibration study carried out with quartz, see Section 2 above, the quality of the diffraction data was assessed using a gypsum sample (powder). A sapphire capillary was filled and powder patterns were collected in static and rotating modes (see Fig. 5). It can be seen that the static pattern presents signatures of texture but, because it is a single-phase sample, with relatively small particle size, the static pattern yields relatively smooth Debye–Scherrer arches. These data were processed for the five patterns recorded at different positions, as described in Section 2 (first radial integration, then summation), to yield the one-dimensional powder patterns (see Fig. 6).

The diffraction peak shapes for the gypsum pattern recorded under spinning were slightly better (more symmetric) than those recorded in static conditions. However, it was concluded that the quality of the statically acquired data was good enough for structural studies. The resolution (diffraction peak width) of both data sets is determined by the internal diameter of the used capillary. For the same experimental configuration, narrower capillaries will yield narrower diffraction peaks.

The synchrotron powder patterns of the anhydrous oil well cement at room pressure, static and under spinning, were also recorded for completeness. The raw data images are shown in Fig. S8. For the static pattern, it can be seen that many Debye–Scherrer arches are grainy, which is due to the large particle size of the alite phase (Ca_3SiO_5), the main component of the cement, and the low amount of minor phases, which does not ensure random diffracting particles in all directions.

The high-pressure and high-temperature experiment started with the preparation of the cement slurry as described in Section 2. This slurry was injected into the sapphire tube using a syringe connected with a short piece of silicone tubing. The tubing was then fitted to the capillary assembly, taking care to avoid the introduction of air bubbles. Then, two PTFE cylindrical pieces, described in Section 2, were placed at both sides of the slurry to avoid oil contamination along the hydration reaction. These plugs also prevented migration of the slurry to other parts of the cell.

After loading cement slurry into the capillary, the cell was closed and oil was pumped into both ends of the system to attain the target pressure. For this experiment, the pressure was set to 150 bar. The measurements were fully consistent in the three pressure evaluation systems, two in the pressure generator and one in the exchange chamber. Once the target pressure was stable, a cell-spinning powder pattern was recorded. All the steps, from cement slurry preparation to the collection of the first pattern, took 55 min. However, this procedure is under optimization and the first data set can be recorded in less than 30 min. Then, the temperature was increased to 150°C. This sequence was chosen because the effect of temperature is larger than that of pressure in cement hydration (Jupe *et al.*, 2011, 2012).

In situ synchrotron X-ray powder diffraction patterns were recorded every 15 min. The full experiment lasted 15 h for studying cement hydration up to a large degree of reaction of the different phases in these conditions. The quantitative analysis of all data including the sequences of the reactions will be reported elsewhere. Here, we focus on the quantitative analysis of one pattern to highlight the improvement achieved by the use of a spinning cell. The 2D raw data for the cement slurry hydrated for 14 h (13 h under 150 bar and 150°C) are

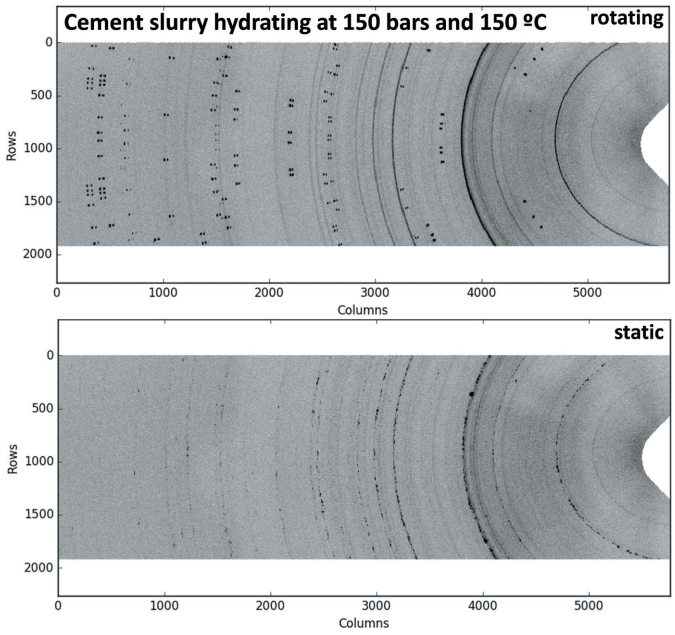

Figure 7
In situ 2D synchrotron powder diffraction patterns of the hydrating cement slurry, 14 h of hydration, at 150 bar and 150°C: (top) under rotation and (bottom) static.

displayed in Fig. 7. This figure compares the patterns collected in static spinning modes. The static pattern is very grainy, which leads to poor peak shapes of the diffraction peaks and inaccurate intensities after radial integration. This is shown in Fig. 8, where selected diffraction peaks are shown for the five positions of the capillary and for the two modes: rotating and static. The smooth rings obtained under rotation, when radially integrated, yield reproducible peak shapes and

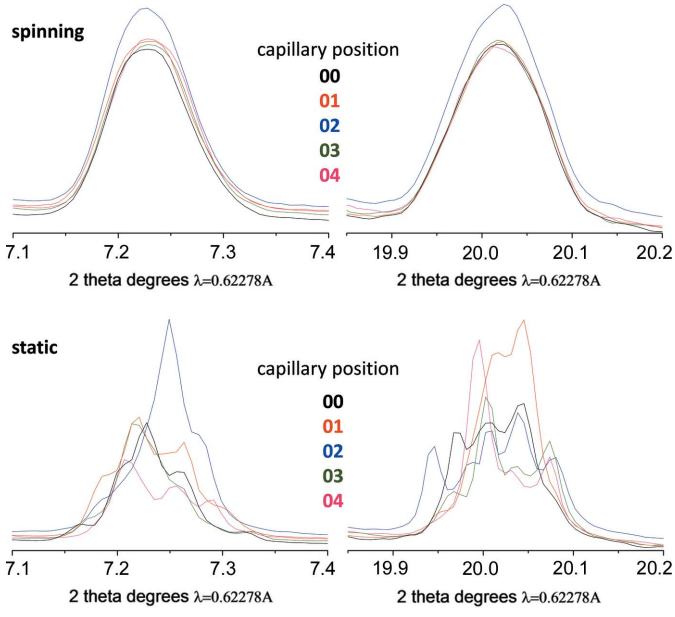

Figure 8
Comparison of the 1D synchrotron powder diffraction peaks at five capillary positions, after radial integration, for hydrating cement slurry at 14 h: (top) rotating and (bottom) static.

Table 1
Selected details for the RQPA of the oil well cement slurry after 14 h of hydration under 150 bar and 150°C.

Phase	Content (wt%)	R_F (%)	ICSD code
$Ca_3SiO_5 - M_3$	4.1 (3)	14.8	94742
$Ca_2SiO_4 - \beta$	15.7 (3)	13.4	81096
Ca_2AlFeO_5	22.0 (2)	9.1	9197
$Ca(OH)_2$	35.0 (1)	3.2	15471
$Ca_2SiO_4{\cdot}H_2O - \alpha$	5.6 (3)	16.1	73404
Katoite	16.7 (2)	8.3	49772
Jaffeite	0.8 (2)	19.8	39725

intensities. Conversely, the grainy rings recorded in the static capillary, when integrated, result in variable peak shapes and intensities. This is partly mitigated when summing up the five 1D patterns, but the resulting powder pattern still presents asymmetric diffraction peak shapes. Larger 2D detectors would improve the particle statistics with 2θ as larger fractions of the Debye–Scherrer rings are collected. For the 2D detector used in this work, the fraction of the recorded reflection changes with the diffracting angle. Fig. S9 reports the evolution of selected single peak integrations with 2θ.

The five powder patterns collected under spinning at 14 h of hydration were summed with local software, to yield the final data set that was fitted by the Rietveld method. Fig. 9 shows the synchrotron Rietveld plot after the analysis. This fit does not take into account the amorphous phases, and the signals from the sapphire capillary were masked. The RQPA results are reported in Table 1. It is highlighted that α-$Ca_2SiO_4{\cdot}H_2O$ and Jaffeite phases are only obtained in cement hydration at high pressures (Meller *et al.*, 2007; Palou *et al.*, 2014; Kuzielová *et al.*, 2017).

The quality of the quantitative phase analysis is judged to be very good based on two observations. Firstly, the difference curve (see bottom blue line in Fig. 9) is quite flat, reflecting a good agreement between the measured (crosses) and calculated (red line) patterns. Secondly, and very importantly, the R_F factors are quite low. For a detailed discussion of *R*-factors in the Rietveld fits, the reader is referred to publications dealing with this topic (*e.g.* McCusker *et al.*, 1999; Toby, 2006).

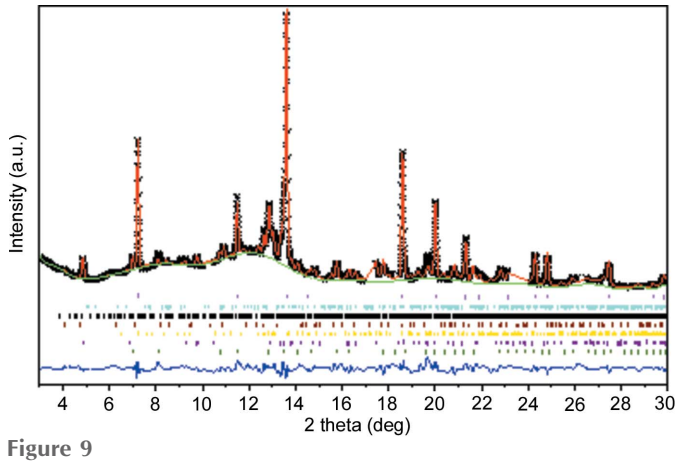

Figure 9
In situ 1D Rietveld synchrotron powder diffraction plot for the oil well cement slurry after 14 h of hydration under 150 bar and 150°C.

Here, we highlight that R_F factors are phase-dependent and they are low if the chosen structural descriptions are adequate and the powder diffraction data do not have systematic errors. As expected, low-content phases displayed larger R_F factors.

4. Conclusions

This new spinning capillary cell has been successfully operated up to 200 bar and 200°C. It has been designed to reduce the stress into the capillary imposed by the rotation torque. Furthermore, the improvement in powder diffraction data quality is obvious and has allowed an *in situ* Rietveld quantitative phase analysis of a hydrating oil well cement at 150 bar and 150°C. The cell is now open to users but through collaboration with ALBA staff.

5. Outlook

The pressure limit of the cell has not been reached so far. Under 200 bar and with a speed limit of 250 r.p.m., no capillary has been broken as yet, in all tests. It will be interesting in the future to reach pressures close to 500 bar. Some modifications are needed in order to reach this goal, especially in the rotating PTFE seals and some fittings attached to the side supports. Other possible improvement would be a more compact design which would allow the cell to be implemented in laboratory X-ray powder diffractometers with molybdenum radiation (León-Reina *et al.*, 2016). This compact design allows the cell to be used in confined spaces. Furthermore, it would fit within Eulerian cradles present in many synchrotron powder diffractometers. In this case, very high resolution powder patterns will be collected as the multicrystal analyser setups could be used. This configuration will profit most from the performances of this cell as point detectors will be employed.

Acknowledgements

The design, production and commissioning of this cell was carried out at the ALBA synchrotron as part of Edmundo Fraga's PhD project. We are grateful to Professor Angus Wilkinson, Georgia Institute of Technology Atlanta, for sharing his knowledge and details on the high pressure cell developed by his team. We also thank Dr Marcus Paul, Dyckerhoff-Lengerich, Germany, for fruitful discussion on oil well cements. The cell was commissioned at the BL11-NCD-SWEET beamline.

Funding information

This work was financially supported by the Spanish Ministry of Economy and Competitiveness through Grants BIA2014-57658-C2-1-R and BIA2017-82391-R which are co-funded by FEDER.

References

Aranda, M. A. G. (2016). *Crystallogr. Rev.* **22**, 150–196.
Ashiotis, G., Deschildre, A., Nawaz, Z., Wright, J. P., Karkoulis, D., Picca, F. E. & Kieffer, J. (2015). *J. Appl. Cryst.* **48**, 510–519.
Azhdari, A., Nemat-Nasser, S. & Rome, J. (1998). *Int. J. Fract.* **94**, 251–266.
Beek, W. van & Pattison, P. (2018). *International Tables for Crystallography*, Vol. H, edited by C. J. Gilmore, J. A. Kaduk & H. Schenk, ch. 2.9, pp. 189–192. International Union of Crystallography.
Chupas, P. J., Chapman, K. W., Kurtz, C., Hanson, J. C., Lee, P. L. & Grey, C. P. (2008). *J. Appl. Cryst.* **41**, 822–824.
González, J. B., González, N., Colldelram, C., Ribó, L., Fontserè, A., Jover-Manas, G., Villanueva, J., Llonch, M., Peña, G., Gevorgyan, A., Nikitin, Y., Martínez, J. C., Kamma-Lorger, C., Solano, E., Sics, I., Ferrer, S. & Malfois, M. (2018). *Proceedings of the 10th Mechanical Engineering Design of Synchrotron Radiation Equipment and Instrumentation (MEDSI2018)*, 25–29 June 2018, Paris, France, pp. 374–376. THPH17.
Hansen, B. R. S., Møller, K. T., Paskevicius, M., Dippel, A.-C., Walter, P., Webb, C. J., Pistidda, C., Bergemann, N., Dornheim, M., Klassen, T., Jørgensen, J.-E. & Jensen, T. R. (2015). *J. Appl. Cryst.* **48**, 1234–1241.
Ida, T., Goto, T. & Hibino, H. (2009). *J. Appl. Cryst.* **42**, 597–606.
Jensen, T. R., Nielsen, T. K., Filinchuk, Y., Jørgensen, J.-E., Cerenius, Y., Gray, E. M. & Webb, C. J. (2010). *J. Appl. Cryst.* **43**, 1456–1463.
Jupe, A. C. & Wilkinson, A. P. (2006). *Rev. Sci. Instrum.* **77**, 113901.
Jupe, A. C., Wilkinson, A. P. & Funkhouser, G. P. (2011). *J. Am. Ceram. Soc.* **94**, 1591–1597.
Jupe, A. C., Wilkinson, A. P. & Funkhouser, G. P. (2012). *Cem. Concr. Res.* **42**, 1083–1087.
Kuzielová, E., Žemlička, M., Másilko, J. & Palou, M. T. (2017). *Geothermics*, **68**, 86–93.
León-Reina, L., García-Maté, M., Álvarez-Pinazo, G., Santacruz, I., Vallcorba, O., De la Torre, A. G. & Aranda, M. A. G. (2016). *J. Appl. Cryst.* **49**, 722–735.
McCusker, L. B., Von Dreele, R. B., Cox, D. E., Louër, D. & Scardi, P. (1999). *J. Appl. Cryst.* **32**, 36–50.
Meller, N., Hall, C., Kyritsis, K. & Giriat, G. (2007). *Cem. Concr. Res.* **37**, 823–833.
Palou, M., Živica, V., Ifka, T., Boháč, M. & Zmrzlý, M. (2014). *J. Therm. Anal. Calorim.* **116**, 597–603.
Sakaki, K., Kim, H., Machida, A., Watanuki, T., Katayama, Y. & Nakamura, Y. (2018). *J. Appl. Cryst.* **51**, 796–801.
Thompson, P., Cox, D. E. & Hastings, J. B. (1987). *J. Appl. Cryst.* **20**, 79–83.
Toby, B. H. (2006). *Powder Diffr.* **21**, 67–70.
Von Dreele, R. B. & Larson, A. C. (2004). *Los Alamos Natl. Lab. Rep. LAUR.* **748**, 86–748.